# Migration velocity analysis for anisotropic models

*Yunyue (Elita) Li and Biondo Biondi*

## ABSTRACT

Anisotropic models are recognized as more realistic representations of the subsurface in complex geological environments. These models are widely needed by many kinds of migration and interpretation schemes. However, anisotropic model building is still a challenging problem in the industry. In this paper, we propose an approach to building anisotropic models from surface seismic data based on the theory of Wave-Equation Migration Velocity Analysis (WEMVA). Because of the ambiguity between depth and Thomsen parameter $\delta$, we parametrize our model space using only NMO velocity ($V_{nmo}$) and the anellipticity parameter $\eta$. We tested the anisotropic WEMVA on a shallow part of the Hess synthetic VTI model. The results show that anisotropic WEMVA is effective in resolving some of the anisotropic perturbation. However, a unique solution to the inversion requires additional constraining information.

## INTRODUCTION

Since first reported in exploration seismology in the 1930s (McCollum and Snell, 1932), anisotropy has become increasingly important in seismic imaging and exploration. Until now, the transverse isotropic (TI) model has been the most commonly used model in seismic imaging. Postma (1955), Helbig (1956) and Backus (1962) have shown that a sequence of isotropic layers on a scale much smaller than the wavelength leads to an anisotropic medium. If the layers are horizontal, the medium is defined as a vertical TI (VTI) medium. A VTI medium is commonly formed because of thin bedding during deposition. If the layers become dipping due to deformation, a tilted TI (TTI) medium is formed. Many authors (Shan, 2009; Fletcher et al., 2009; Zhang and Zhang, 2009; Fei and Liner, 2008) have developed migration and processing schemes for VTI and TTI media; however, the challenge of estimating the anisotropy model remains a bottleneck for the exploration workflow.

The existing anisotropic model-building schemes are mostly based on measuring the non-hyperbolic moveout along the traveltime curve to flatten the common image gathers (CIG) (Zhou et al., 2003, 2004; Yuan et al., 2006; Cai et al., 2009; Woodward et al., 2008). However, traveltime ray-based methods are prone to errors and unrealistic results when multi-pathing exists in areas of complex overburden. Hence, we propose to apply wave-equation tomography for anisotropic model building.

Wave-equation tomography has been widely studied in isotropic velocity building and can be implemented either in the data space, commonly known as Full-Waveform Inversion (FWI) (Tarantola, 1984; Woodward, 1992) or in the image space, commonly known as Wave-Equation Migration Velocity Analysis (WEMVA) (Sava and Biondi, 2004a,b; Shen, 2004; Shen and Symes, 2008; Guerra et al., 2009). Several advantages drive us to use the image-space wave-equation tomography instead of data-space wave-equation tomography: first, WEMVA does not require as accurate an initial model to avoid the cycle-skipping problem as FWI requires. In fact, many studies (Guerra et al., 2009; Guerra and Biondi, 2010; Tang and Biondi, 2010) show that the resolution gap between ray-based tomography and FWI could be linked by the image-space WEMVA method; second, the objective function is directly related to the final image; third, the migrated image is often much cleaner than the recorded wavefields. Therefore, we choose to extend image-space WEMVA from isotropic velocity building to anisotropic model building.

In this paper, we first generalize the methodology of image-space WEMVA from an isotropic medium to an anisotropic medium and explain our parameterization. We show that the gradient of the tomographic objective functional for an isotropic medium can be modified to describe an anisotropic medium by simply adding a term for the additional parameter. Finally, we test our inversion scheme on a shallow part of the Hess anisotropic synthetic dataset.

## MIGRATION VELOCITY ANALYSIS FOR ANISOTROPIC PARAMETERS

Anisotropic MVA is a non-linear inversion process that aims to find the background anisotropic model that minimizes the residual image $\Delta\mathbf{I}$. The residual image is derived from the background image $\mathbf{I}$, which is computed with the current background model. To form the image, both the source and receiver wavefields are downward continued using the one-way wave equations. Assuming that the shear velocity is much smaller than the P-wave velocity, one way of formulating up-going and down-going one-way acoustic wave equations for VTI is shown as follows (Shan, 2009):

$$\left(\frac{\partial}{\partial z} \mp i\Lambda\right) P = 0, \tag{1}$$

where $P = P(x, y, z, \omega)$ is the wavefield in the space-frequency domain and $\Lambda$ describes the dispersion relationship in terms of P-wave vertical slowness $s_0$ and Thomsen parameters $\epsilon$ and $\delta$ (Thomsen, 1986):

$$\Lambda = \omega s_0 \sqrt{\frac{\omega^2 s_0^2 - (1+2\epsilon)|\mathbf{k}|^2}{\omega^2 s_0^2 - 2(\epsilon-\delta)|\mathbf{k}|^2}}, \tag{2}$$

where $\mathbf{k} = (k_x, k_y)$ is the spatial wavenumber vector.

Many authors (Tsvankin and Thomsen, 1994; Alkhalifah and Tsvankin, 1995) have shown that P-wave traveltime can be characterized by the NMO slowness, $s_n$, and the anellipticity parameter $\eta$. Therefore, the one-way wave-equation in terms of $s_n$, $\eta$ and $\delta$ is:

$$\left(\frac{1}{\sqrt{1+2\delta}}\frac{\partial}{\partial z} \mp i\Lambda'\right) P = 0 \tag{3}$$

where

$$\Lambda' = \omega s_n \sqrt{1 - \frac{|\mathbf{k}|^2}{\omega^2 s_n^2 - 2\eta|\mathbf{k}|^2}}. \tag{4}$$

Notice that in the dispersion relationship in Equation 3, $\delta$ and the derivative in depth $\frac{\partial}{\partial z}$, are coupled with each other. This is a theoretical proof of the well-accepted observation that $\delta$ cannot be determined by the surface seismic data. To constrain this parameter, we need well information (e.g. checkshots) to add the depth dimension into the inversion. Now, if we apply the change of variables

$$d\bar{z} = \sqrt{1+2\delta}dz \tag{5}$$

and neglect the derivatives of $\delta$, Equation 3 becomes

$$\left(\frac{\partial}{\partial \bar{z}} \mp i\Lambda'\right) P = 0. \tag{6}$$

We can therefore formulate the image-space migration velocity analysis problem with NMO slowness $s_n$ and anisotropic parameters $\eta$ and $\delta$, but we invert only for $s_n$ and $\eta$ assuming $\delta$ model is known from other source of information.

Notice that when $\eta = 0$, the dispersion relationship ( equation 4) is the same as the isotropic dispersion relationship, and the corresponding one-way wave equation ( equation 6) is almost the same as for the isotropic case, except for a depth stretch caused by $\delta$. In other words, an elliptic anisotropic wavefield inversion is almost equivalent to an isotropic wavefield inversion. Plessix and Rynja (2010) reached the same conclusions for full-waveform inversion (FWI). Figure 1 compares the original NMO velocity to the stretched NMO velocity. Notice that the geological features are stretched downward for positive $\delta$. Because we ignore $\delta$ in the inversion, we expect the inverted NMO velocity to have more similarity to the stretched NMO velocity than to the original one.

In general, the residual image is defined as (Biondi, 2008)

$$\Delta\mathbf{I} = \mathbf{I} - \mathbf{F}(\mathbf{I}), \tag{7}$$

where $\mathbf{F}$ is a focusing operator. In the least-square sense, the tomographic objective function can be written as follows:

$$J = \frac{1}{2}||\Delta\mathbf{I}||_2 = \frac{1}{2}||\mathbf{I} - \mathbf{F}(\mathbf{I})||^2. \tag{8}$$

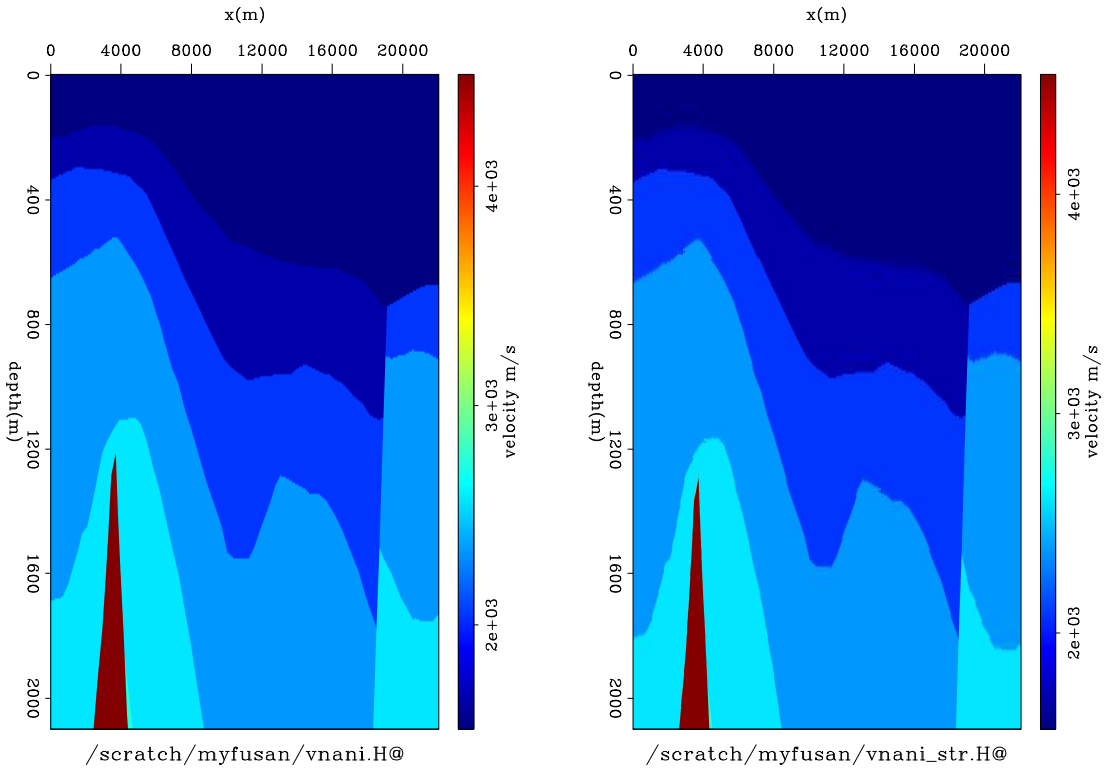


Figure 1: (a) Original NMO velocity for the anisotropic Hess model; (b) Stretched NMO velocity according to $\delta$. The overlaid box denotes the part of model that we work on in the numerical test. [**CR**]

To perform MVA for anisotropic parameters, we first need to extend the tomographic operator from the isotropic medium (Shen, 2004; Sava, 2004; Guerra et al., 2009) to the anisotropic medium. We define the wave-equation tomographic operator $\mathbf{T}$ for anisotropic models as follows:

$$\begin{aligned} \mathbf{T} &= \left.\frac{\partial \mathbf{I}}{\partial \mathbf{m}}\right|_{\mathbf{m}=\widehat{\mathbf{m}}} \\ &= \left.\frac{\partial \mathbf{I}}{\partial \mathbf{s_n}}\right|_{\mathbf{s_n}=\widehat{\mathbf{s_n}}} + \left.\frac{\partial \mathbf{I}}{\partial \eta}\right|_{\eta=\widehat{\eta}} \end{aligned} \tag{9}$$

where $\mathbf{m}$ is the anisotropy model, which in this case includes NMO slowness $\mathbf{s_n}$ and anellipticity parameter $\eta$; $\widehat{\mathbf{m}}$ is the background anisotropy model, consisting of the background NMO slowness $\widehat{\mathbf{s_n}}$ and background anellipticity $\widehat{\eta}$; and $\mathbf{I}$ is the image. This wave equation tomographic operator $\mathbf{T}$ is a linear operator that relates the model perturbation $\Delta\mathbf{m}$ to the image perturbation $\Delta\mathbf{I}$ as follows:

$$\Delta\mathbf{I} = \mathbf{T}\Delta\mathbf{m}. \tag{10}$$

In the shot-profile domain, both source and receiver wavefields are downward continued using the one-way wave equation (6):

$$\begin{cases} \left(\frac{\partial}{\partial z} + i\Lambda'\right) D(\mathbf{x}, \mathbf{x}_s) = 0 \\ D(x, y, z=0, \mathbf{x}_s) = f_s \delta(\mathbf{x} - \mathbf{x}_s) \end{cases}, \tag{11}$$

and

$$\begin{cases} \left(\frac{\partial}{\partial z} + i\Lambda'\right) U(\mathbf{x}, \mathbf{x}_s) = 0 \\ U(x, y, z=0, \mathbf{x}_s) = Q(x, y, z=0, \mathbf{x}_s) \end{cases}, \tag{12}$$

where $D(\mathbf{x}, \mathbf{x}_s)$ is the source wavefield at the image point $\mathbf{x} = (x, y, z)$ with the source located at $\mathbf{x}_s = (x_s, y_s, 0)$; $U(\mathbf{x}, \mathbf{x}_s)$ is the receiver wavefield at the image point $\mathbf{x}$ with the source located at $\mathbf{x}_s$; $f_s$ is the source signature, and $f_s\delta(\mathbf{x} - \mathbf{x}_s)$ defines the point-source function at $\mathbf{x_s}$, which serves as the boundary condition of equation 11; and $Q(x, y, z=0, \mathbf{x}_s)$ is the recorded shot gather for the shot located at $\mathbf{x}_s$, which serves as the boundary condition of equation 12.

The dispersion relationship in equation (4) can be approximated with a rational function by Taylor series and Padé expansion analysis (Shan, 2009):

$$\Lambda' = \omega s_n \left(1 - \frac{a|\mathbf{k}|^2}{\omega^2 s_n^2 - b|\mathbf{k}|^2}\right), \tag{13}$$

where, to the second order of the expansion, $a = 0.5, b = 0.25 + 2\eta$. Equation (13) using binomial expansion can be further expanded to polynomials:

$$\Lambda' = \omega s_n - \frac{a}{\omega^2 s_n^2}|\mathbf{k}|^2 - \frac{ab}{\omega^4 s_n^4}|\mathbf{k}|^4. \tag{14}$$

Now it is straightforward to take the derivative of $\Lambda'$ with respect to $s_n$ and $\eta$.

The background image is computed by applying the cross-correlation imaging condition:

$$I(\mathbf{x},\mathbf{h}) = \sum_{\mathbf{x}_s}\sum_{\omega} \overline{D(\mathbf{x}-\mathbf{h},\mathbf{x}_s)}U(\mathbf{x}+\mathbf{h},\mathbf{x}_s), \tag{15}$$

where the overline stands for complex conjugate, and $\mathbf{h} = (h_x, h_y, h_z)$ is the subsurface half-offset. Perturbing the wavefields in equation (15) and ignoring the higher-order term, we can get the perturbed image as follows:

$$\begin{aligned}\Delta I(\mathbf{x},\mathbf{h}) &= \sum_{\mathbf{x}_s}\sum_{\omega} \Big(\overline{\Delta D(\mathbf{x}-\mathbf{h},\mathbf{x}_s)}\widehat{U}(\mathbf{x}+\mathbf{h},\mathbf{x}_s)+ \\ &\quad \overline{\widehat{D}(\mathbf{x}-\mathbf{h},\mathbf{x}_s)}\Delta U(\mathbf{x}+\mathbf{h},\mathbf{x}_s)\Big),\end{aligned} \tag{16}$$

where $\widehat{D}(\mathbf{x}-\mathbf{h},\mathbf{x}_s)$ and $\widehat{U}(\mathbf{x}+\mathbf{h},\mathbf{x}_s)$ are the background source and receiver wavefields computed with the background model $\widehat{m}(\mathbf{x})$; and $\Delta D(\mathbf{x}-\mathbf{h},\mathbf{x}_s)$ and $\Delta U(\mathbf{x}+\mathbf{h},\mathbf{x}_s)$ are the perturbed source wavefield and perturbed receiver wavefield, which are the results of the model perturbation $\Delta m(\mathbf{x})$.

To evaluate the adjoint tomographic operator $\mathbf{T}^*$, which maps from the image perturbation to the model perturbation, we first compute the wavefield perturbation from the image perturbation using the adjoint imaging condition:

$$\begin{aligned}\Delta D(\mathbf{x},\mathbf{x}_s) &= \sum_{\mathbf{h}} \Delta I(\mathbf{x},\mathbf{h})\widehat{U}(\mathbf{x}+\mathbf{h},\mathbf{x}_s) \\ \Delta U(\mathbf{x},\mathbf{x}_s) &= \sum_{\mathbf{h}} \Delta I(\mathbf{x},\mathbf{h})\widehat{D}(\mathbf{x}-\mathbf{h},\mathbf{x}_s).\end{aligned} \tag{17}$$

The perturbed source and receiver wavefields satisfy the following one-way wave equations, linearized with respect to NMO slowness and $\eta$:

$$\begin{cases} \left(\frac{\partial}{\partial z} + i\Lambda'\right)\Delta D(\mathbf{x},\mathbf{x}_s) = \left(-i\frac{\partial\Lambda'}{\partial\mathbf{m}}\widehat{D}(\mathbf{x},\mathbf{x}_s)\right)\Delta\mathbf{m}^*(\mathbf{x}) \\ \Delta D(x,y,z=0,\mathbf{x}_s) = 0 \end{cases}, \tag{18}$$

and

$$\begin{cases} \left(\frac{\partial}{\partial z} + i\Lambda'\right)\Delta U(\mathbf{x},\mathbf{x}_s) = \left(-i\frac{\partial\Lambda'}{\partial\mathbf{m}}\widehat{U}(\mathbf{x},\mathbf{x}_s)\right)\Delta\mathbf{m}^*(\mathbf{x}) \\ \Delta U(x,y,z=0,\mathbf{x}_s) = 0 \end{cases}, \tag{19}$$

where $\mathbf{m}$ is the row vector $[\mathbf{s_n}\ \eta]$.

During the inversion, the model perturbation is unknown, and in fact must be estimated. Therefore, we obtain the image perturbation by applying a focusing operator (equation 7) to the current background image. Then the perturbed image is convolved with the background wavefields to get the perturbed wavefields (equation 17). The scattered wavefields are obtained by applying the adjoint of the one-way wave-equations (18) and (19). Finally, the model-space gradient is obtained by cross-correlating the upward propagated scattered wavefields with the modified background wavefields [the terms in the parentheses on the right-hand sides of equations (18) and (19)].

## OBJECTIVE FUNCTION

As mentioned in the previous section, we estimate the optimum earth model by minimizing a user-defined image perturbation. There are many ways to define the objective function. Here we use the Differential Semblance Optimization (DSO) method (Symes and Carazzone, 1991; Shen, 2004) as the criterion:

$$\mathbf{F}(\mathbf{I}) = (\mathbf{1} - \mathbf{O})\mathbf{I}, \tag{20}$$

where $\mathbf{1}$ is the identity operator and $\mathbf{O}$ is the differential operator along the angle axes in the ADCIGs $\mathbf{I}$. In the subsurface-offset domain, the objective function (Equation 8) reads:

$$J = \frac{1}{2}||h\mathbf{I}(\mathbf{x}, \mathbf{h})||_2, \tag{21}$$

where $h$ is the absolute value of subsurface-offset, and $\mathbf{I}(\mathbf{x}, \mathbf{h})$ is the image gather in the subsurface-offset domain. This operator is preferred by many researchers since it is a fully automated procedure, with no picking required. However, for isotropic migration velocity analysis, many authors (Vyas and Tang, 2010; Fei and Williamson, 2010) observe undesired artifacts generated by the DSO operator and suggest that a differential operator along $h$ can help compensate for the phase shift caused by the velocity perturbation. Therefore, we use the modified DSO operator as follows:

$$J = \frac{1}{2}||h\mathbf{D}\mathbf{I}(\mathbf{x}, \mathbf{h})||_2, \tag{22}$$

where $\mathbf{D}$ is a differential operator in $\mathbf{h}$. Taking the derivative in the subsurface offset domain is equivalent to an $\alpha$ weighting in the angle domain. Therefore, the objective function (Equation 22) also emphasizes the contribution of the large angle information, which is crucial for velocity analysis.

To guarantee a smooth inversion, we choose a B-spline representation of the model space. The smoothed gradient in the original space is then represented as:

$$\hat{\mathbf{g}} = \mathbf{B}\mathbf{B}^*\mathbf{g}, \tag{23}$$

where $\mathbf{g}$ and $\hat{\mathbf{g}}$ are the original and the smoothed gradient on the original model grid; $\mathbf{B}$ is the B-spline projection operator. Then the number and spacing of the B-spline nodes control the smoothness of the model update. Practically, we can choose different B-spline parameters for velocity and $\eta$.

## NUMERICAL TEST

We test our inversion scheme on the shallow part of the Hess synthetic anisotropic model, as denoted by the gray square in Figure 1. The initial model is a 1D gradient isotropic model from the seabed. Figure 2 compares the inversion results with the true models. The ratio of intial velocity and inverted velocity over the true stretched

NMO velocity are shown in Figure 2(a) and 2(b), respectively. The error in the initial NMO velocity is up to 25%, which is far beyond the tolerance of FWI. The anisotropic WEMVA successfully reduces the error in velocity down to less than 5%. Notice that the error in velocity generally follows the dip in the image. This suggests that we should use better smoothing operators such as dip (steering) filters (Hale, 2007; Clapp, 2000) to regularize the inversion.

On the other hand, the $\eta$ update [Figure 2(d)] is in general larger than the true $\eta$ model [Figure 2(c)]. A trade-off is observed below 1,600 m, where the inverted velocity is smaller but $\eta$ is much larger than the true values. This result illustrates the null space of our inversion problem, since the reflector around 2,200 m is well-focused (although not perfectly focused) in the final image obtained with the inverted model [Figure 3(b)]. This problem can presumably be resolved by increasing the angle coverage at depth and allowing more iterations in the inversion.

Figure 3 compares the subsurface-offset images using the initial model (a), the updated model (b), and the true model (c). After the inversion, the reflectors are focused at zero subsurface-offset, and the depths of the reflectors are closer to the true depths. The focused image shows that we are dealing with a non-linear problem with a large null space. To reduce the size of the null space, and hence the uncertainty in the inverted model, other information such as checkshots or rock-physics prior knowledge is needed (Li et al., 2011a,b).

## CONCLUSION AND DISCUSSION

We have presented a new methodology for performing image-domain migration velocity analysis in anisotropic media. Our method is a natural extension of isotropic MVA theory and retains the same properties as isotropic MVA. We demostrate our method on a 2-D synthetic data set. After inversion, we obtain better-focused subsurface-offset images and better-defined depths. By including the geological information and the wider-offset data, we should be able to eliminate the model error at depth.

Experience shows that the DSO operator has a layer-stripping effect during the iterations. One cause of this effect is the unbalanced amplitude for the reflectors in depth. Therefore, an illumination-corrected image is preferred to compensate for this effect. On the other hand, a residual-moveout-based objective function (Sava, 2004; Sava and Biondi, 2004a,b; Almomin, 2011; Zhang and Biondi, 2011) could avoid the problem.

Compared with ray-based image-space model-building methods, our wavefield-based image-space method is computationally more intensive. However, the wavefield method better approximates wave propagation in complex areas. We can also utilize the phase-encoded target-oriented image-space wavefield tomography (Guerra et al., 2009; Guerra and Biondi, 2010) technique to reduce the computational cost.

Finally, by introducing another parameter $\eta$ into the MVA inversion, we now have

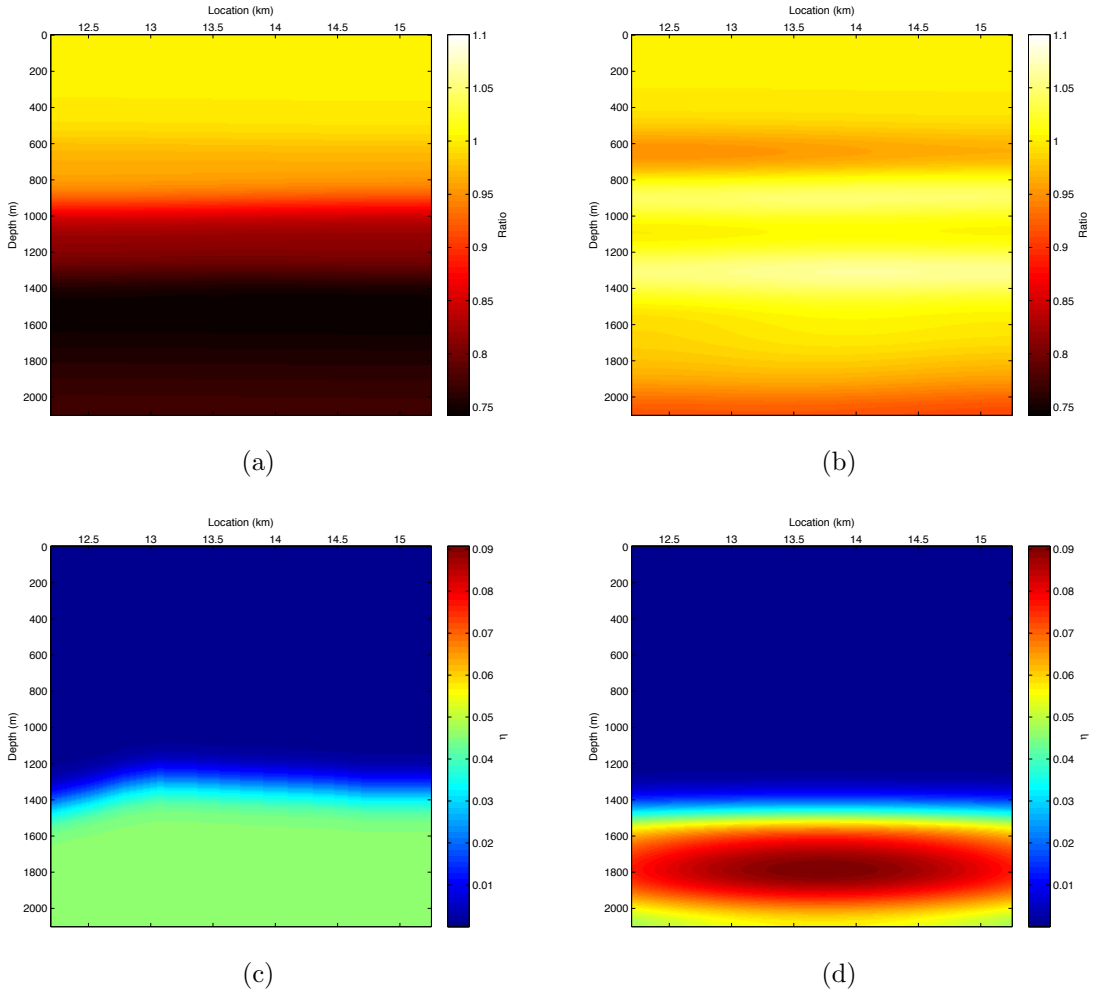


Figure 2: (a) Ratio of initial velocity over true velocity; (b) ratio of inverted velocity over true velocity; (c) true $\eta$ model; (d) inverted $\eta$ model. [**CR**]

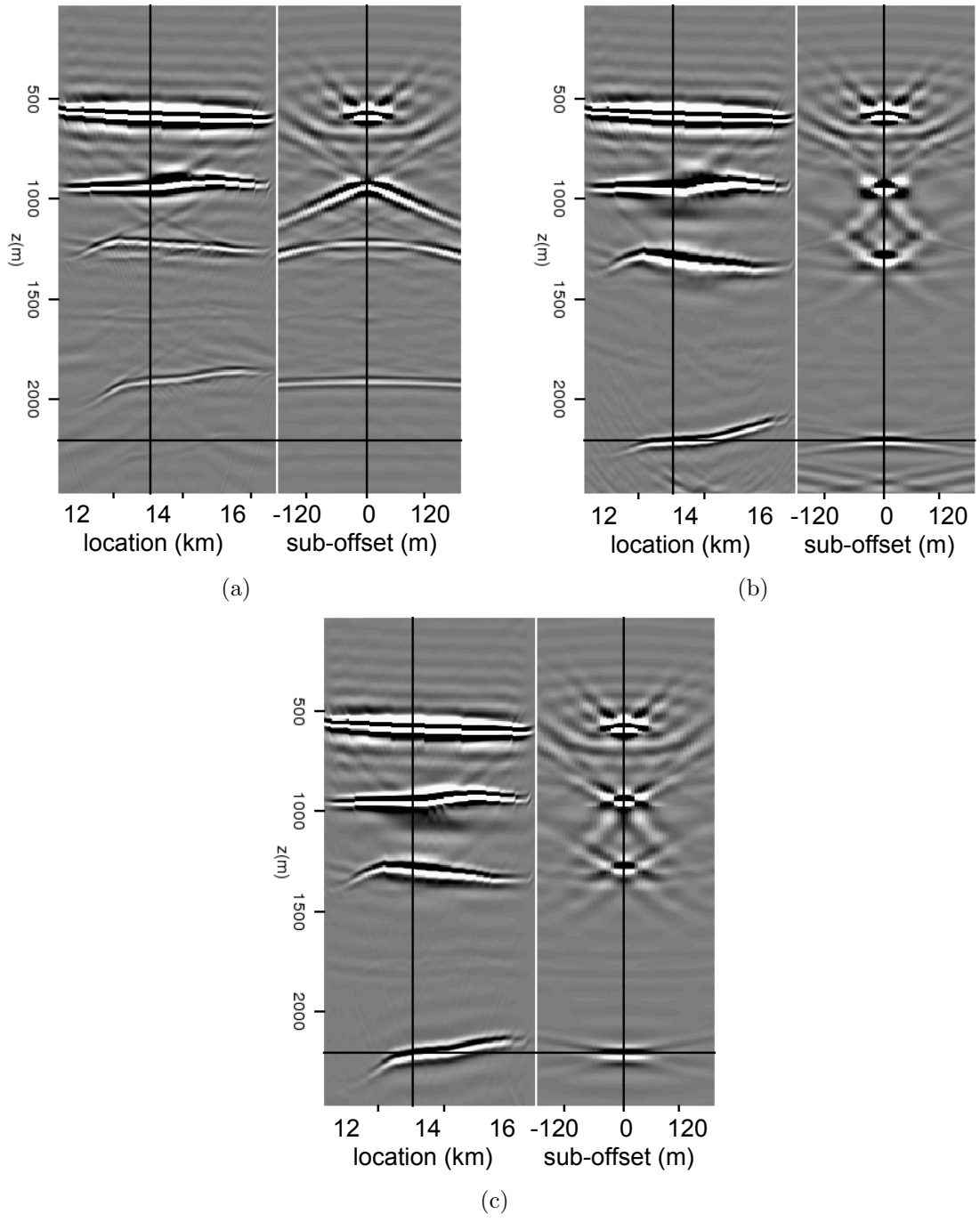


Figure 3: Subsurface offset images using the initial model (a), the updated model (b), and the true model (c). [**CR**]

a larger model space and hence a larger null space with respect to the same data. Therefore, the surface reflection seismic data is inadequate for resolving a unique earth model. Other information, such as borehole measurement, geological interpretation (Bakulin et al., 2010), or rock-physics prior knowledge (Li et al., 2011a,b), is necessary to obtain a consistent, unique and reliable earth model.

## ACKNOWLEDGMENT

We would like to thank James Berryman for fruitful discussions. We thank Hess for providing the Hess anisotropic synthetic dataset.

## REFERENCES

Alkhalifah, T. and I. Tsvankin, 1995, Velocity analysis for transversely isotropic media: Geophysics, **60**, 1550–1566.

Almomin, A., 2011, Correlation-based wave-equation migration velocity analysis: SEP-Report, **143**, 33–42.

Backus, G. E., 1962, Long-wave elastic anisotropy introduced by horizontal layering: J. Geophys. Res., **67**, 4427–4440.

Bakulin, A., M. Woodward, Y. Liu, O. Zdraveva, D. Nichols, and K. Osypov, 2010, Application of steering filters to localized anisotropic tomography with well data: SEG Expanded Abstracts, **29**, 4286–4290.

Biondi, B., 2008, Automatic wave-equation migration velocity analysis: **SEP-134**, 65–78.

Cai, J., Y. He, Z. Li, B. Wang, and M. Guo, 2009, TTI/VTI anisotropy parameters estimation by focusing analysis, Part I: theory: SEG Expanded Abstracts, **28**, 301–305.

Clapp, R., 2000, Geologically constrained migration velocity analysis: PhD thesis, Stanford University.

Fei, T. W. and C. L. Liner, 2008, Hybrid Fourier finite-difference 3D depth migration for anisotropic media: Geophysics, **73**, 27–34.

Fei, W. and P. Williamson, 2010, On the gradient artifacts in migration velocity analysis based on differential semblance optimization: SEG Expanded Abstracts, **29**, 4071–4076.

Fletcher, R., X. Du, and P. J. Fowler, 2009, Stabilizing acoustic reverse-time migration in TTI media: SEG Expanded Abstracts, **28**, 2985–2989.

Guerra, C. and B. Biondi, 2010, Fast 3D velocity updates using the pre-stack exploding reflector model: SEG Expanded Abstract, **29**, 4375–4379.

Guerra, C., Y. Tang, and B. Biondi, 2009, Wave-equation tomography using image-space phase-encoded data: SEP-report, **138**, 95.

Hale, D., 2007, Local dip filtering with directional Laplacians: CWP Report 567.

Helbig, K., 1956, Die ausbreitung elastischer Wellen in anisotropen Medien: Geophys. Prosp., **04**, 70–81.

Li, Y., D. Nichols, K. Osypov, and R. Bachrach, 2011a, Anisotropic tomography using rock physics contraints: Accepted by the proceeding EAGE.

———, 2011b, Anisotropic tomography with rock physics constraints: SEP-Report, **143**, 249–258.

McCollum, B. and F. Snell, 1932, Asymmetry of sound velocity in stratified formations: Physics (Journal of Applied Physics), **2**, 174–185.

Plessix, R.-E. and H. Rynja, 2010, VTI full waveform inversion: a parameterization study with a narrow azimuth streamer data example: SEG Expanded Abstracts, **29**, 962–966.

Postma, G. W., 1955, Wave propagation in a stratified medium: Geophysics, **20**, 780–806.

Sava, P., 2004, Migration and velocity analysis by wavefield extrapolation: PhD thesis, Stanford University.

Sava, P. and B. Biondi, 2004a, Wave-equation migration velocity analysis-I: Theory: Geophysical Prospecting, **52**, 593–606.

———, 2004b, Wave-equation migration velocity analysis-II: Examples: Geophysical Prospecting, **52**, 607–623.

Shan, G., 2009, Optimized implicit finite-difference and Fourier finite-difference migration for VTI media: Geophysics, WCA189–WCA197.

Shen, P., 2004, Wave-equation Migration Velocity Analysis by Differential Semblance Optimization: PhD thesis, Rice University.

Shen, P. and W. W. Symes, 2008, Automatic velocity analysis via shot profile migration: Geophysics, **73**, VE49–VE59.

Symes, W. W. and J. J. Carazzone, 1991, Velocity inversion by differential semblance optimization: Geophysics, **56**, 654–663.

Tang, Y. and B. Biondi, 2010, Target-oriented wavefield tomography using demigrated Born data: SEG Expanded Abstract, **29**, 4280–4285.

Tarantola, A., 1984, Inversion of seismic reflection data in the acoustic approximation: Geophysics, **49**, 1259–1266.

Thomsen, L., 1986, Weak elastic anisotropy: Geophysics, **51**, 1954–1966.

Tsvankin, I. and L. Thomsen, 1994, Nonhyperbolic reflection moveout in anisotropic media: Geophysics, **59**, 1290–1304.

Vyas, M. and Y. Tang, 2010, Gradients for wave-equation migration velocity analysis: SEG Expanded Abstracts, **29**, 4077–4081.

Woodward, M. J., 1992, Wave-equation tomography: Geophysics, **57**, 15–26.

Woodward, M. J., D. Nichols, O. Zdraveva, P. Whitfield, and T. Johns, 2008, A decade of tomography: Geophysics, **73**, VE5–VE11.

Yuan, J., X. Ma, S. Lin, and D. Lowrey, 2006, P-wave tomographic velocity updating in 3D inhomogeneous VTI media: SEG Expanded Abstracts, **25**, 3368–3372.

Zhang, Y. and B. Biondi, 2011, Moveout-based wave-equation migration velocity analysis: SEP-Report, **143**, 43–58.

Zhang, Y. and H. Zhang, 2009, A stable TTI reverse time migration and its implementation: SEG Expanded Abstracts, **28**, 2794–2798.

Zhou, H., D. Pham, and S. Gray, 2004, Tomographic velocity analysis in strongly anisotropic TTI media: SEG Expanded Abstracts, **23**, 2347–2350.

Zhou, H., D. Pham, S. Gray, and B. Wang, 2003, 3-D tomographic velocity analysis in transversely isotropic media: SEG Expanded Abstracts, **22**, 650–653.

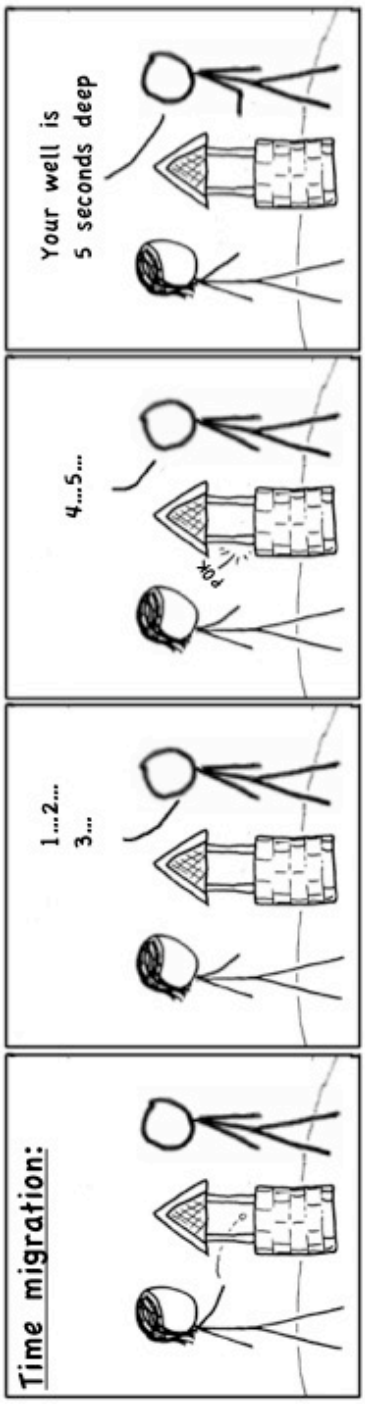
Time migration:
1...2...
3...
4...5...
POK
Your well is
5 seconds deep